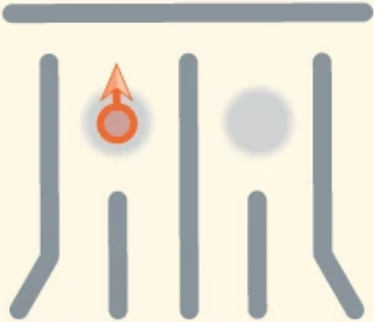
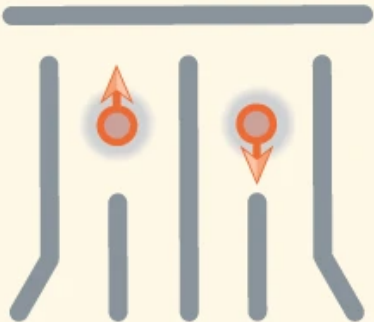


A Singlet-Triplet Hole Spin Qubit in Planar Ge

Jirovec, D., Hofmann, A., Ballabio, A. *et al. Nat. Mater.* **20**, 1106–1112 (2021)

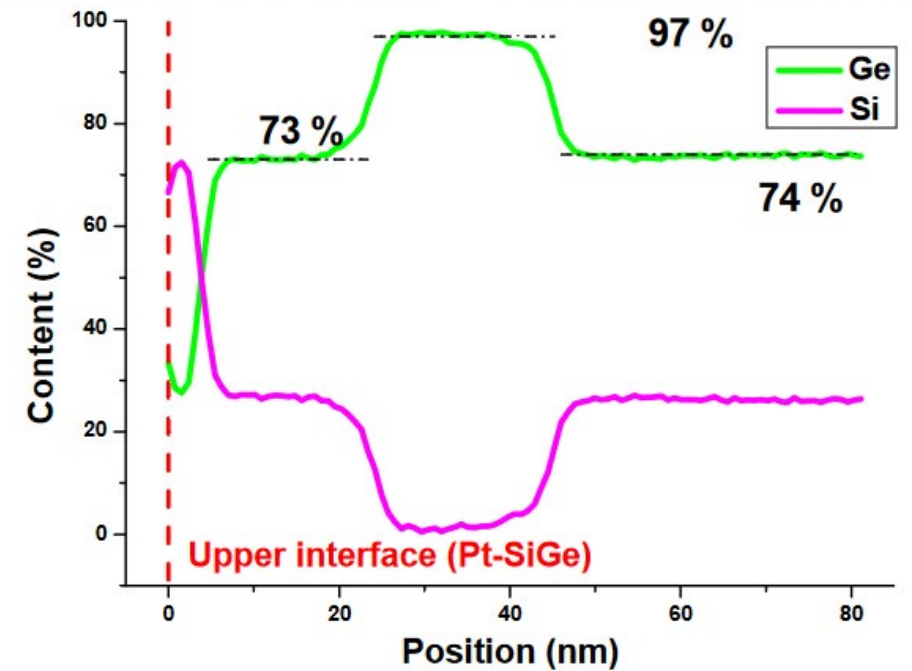
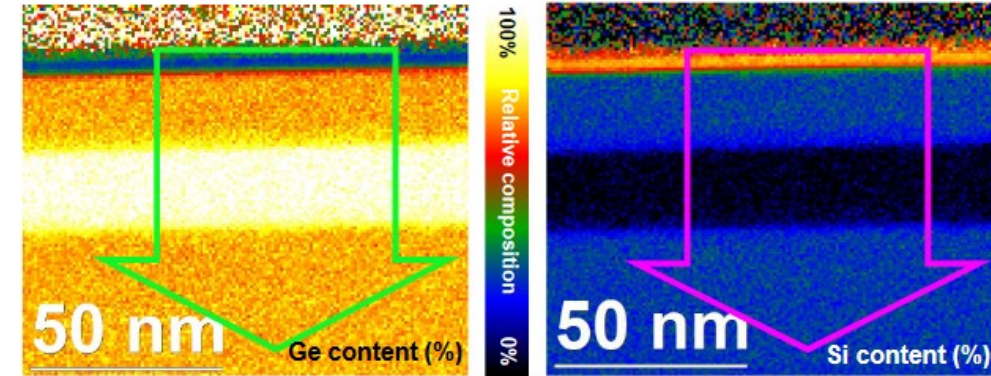
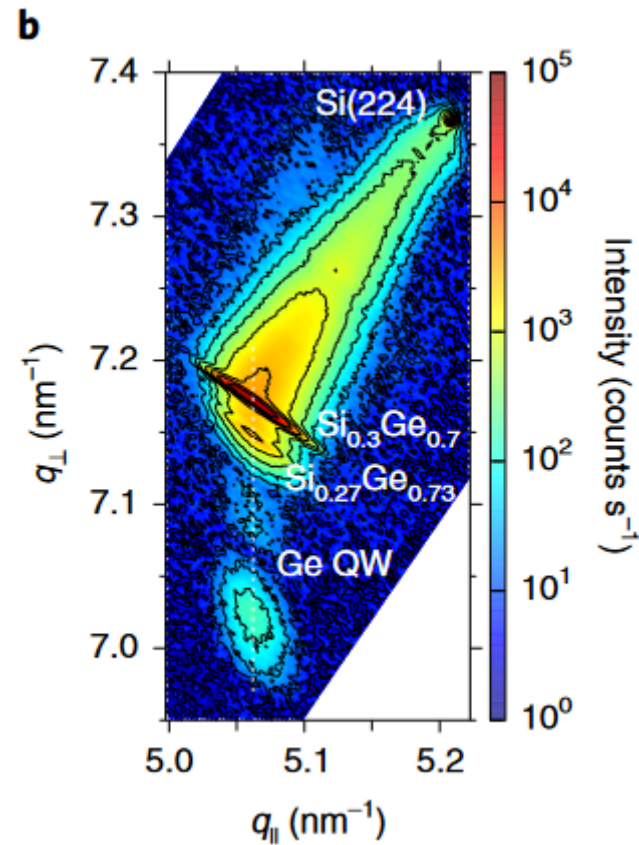
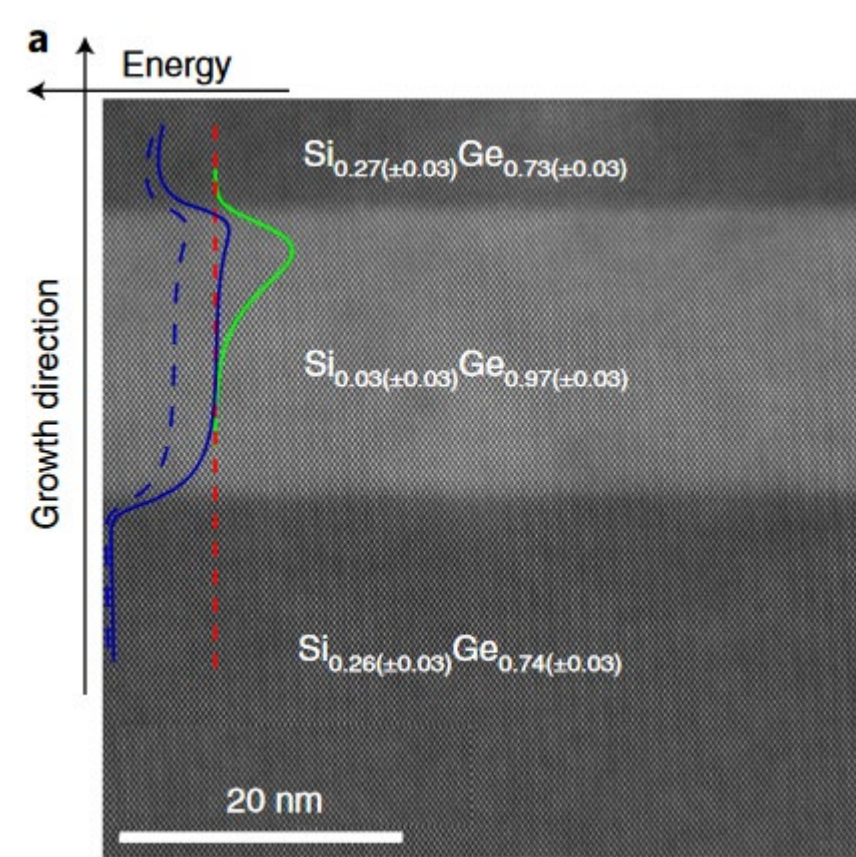
Spin Journal Club, 11.07.22, Eric Jutzi

Encoding Schemes

	Qubit encoding	f_{Rabi} (MHz)	T_2^* (μs)	B (T)	Ref.
LD qubit	 $ 0\rangle : \downarrow\rangle$ $ 1\rangle : \uparrow\rangle$	85	0.06	0.144	2
		140	0.13	0.127	4
		435	0.011	0.206	5
		>100	0.833	1.65	6
		147	0.44	0.3	15
		542	0.082	0.1	16
ST_0 qubit	 $ 0\rangle : \frac{1}{\sqrt{2}} (\uparrow\downarrow\rangle - \downarrow\uparrow\rangle)$ $ 1\rangle : \frac{1}{\sqrt{2}} (\uparrow\downarrow\rangle + \downarrow\uparrow\rangle)$	150	1	<0.01	1

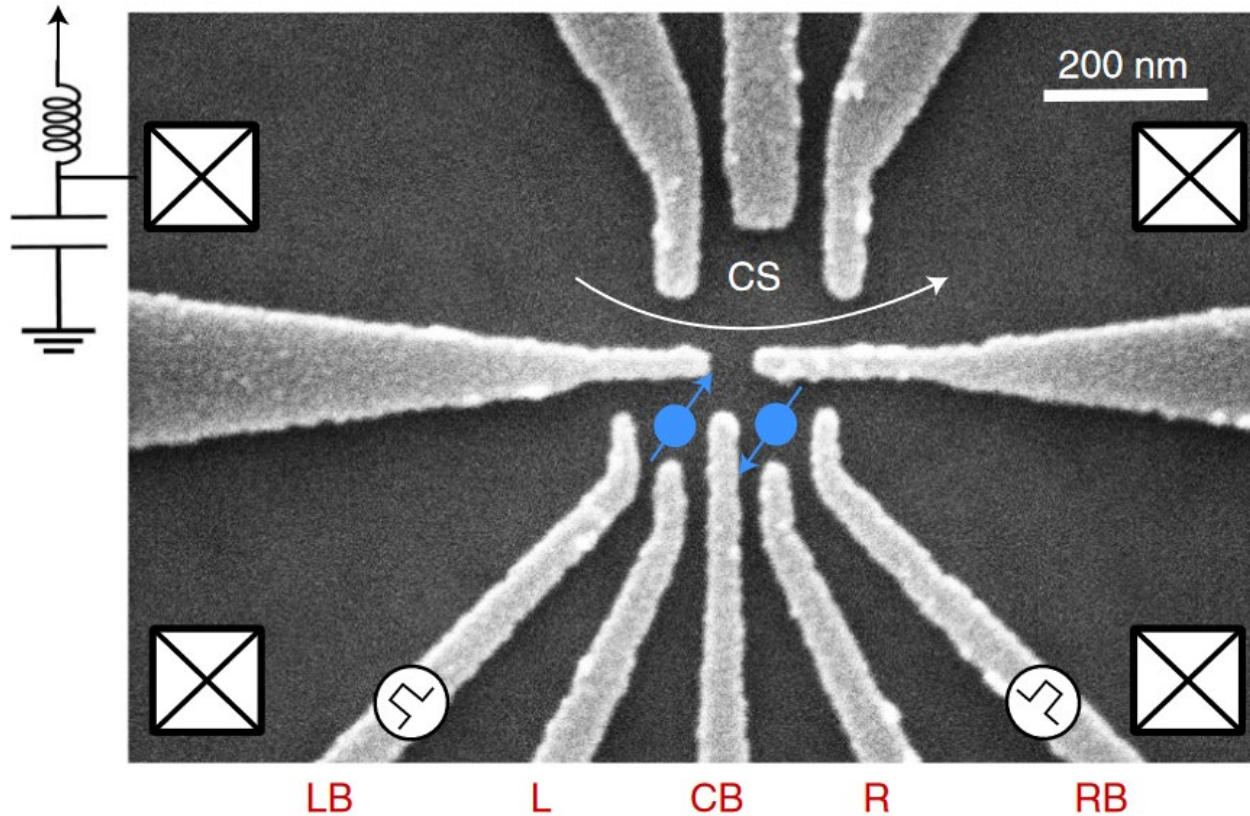
Braakman, F., Scarlino, P. *Nat. Mater.* **20**, 1047–1048 (2021)

The heterostructure



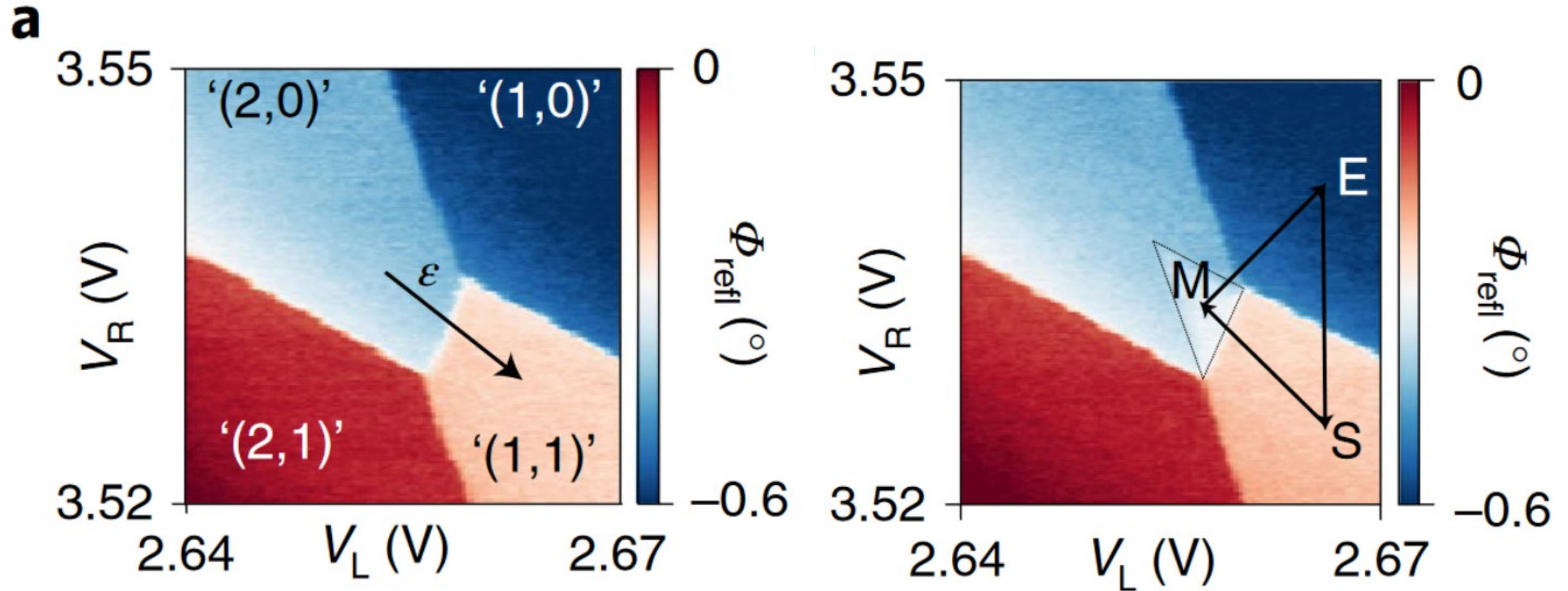
- -0.15 % in-plane in barrier
- -1.18% in-plane in Ge QW

The device

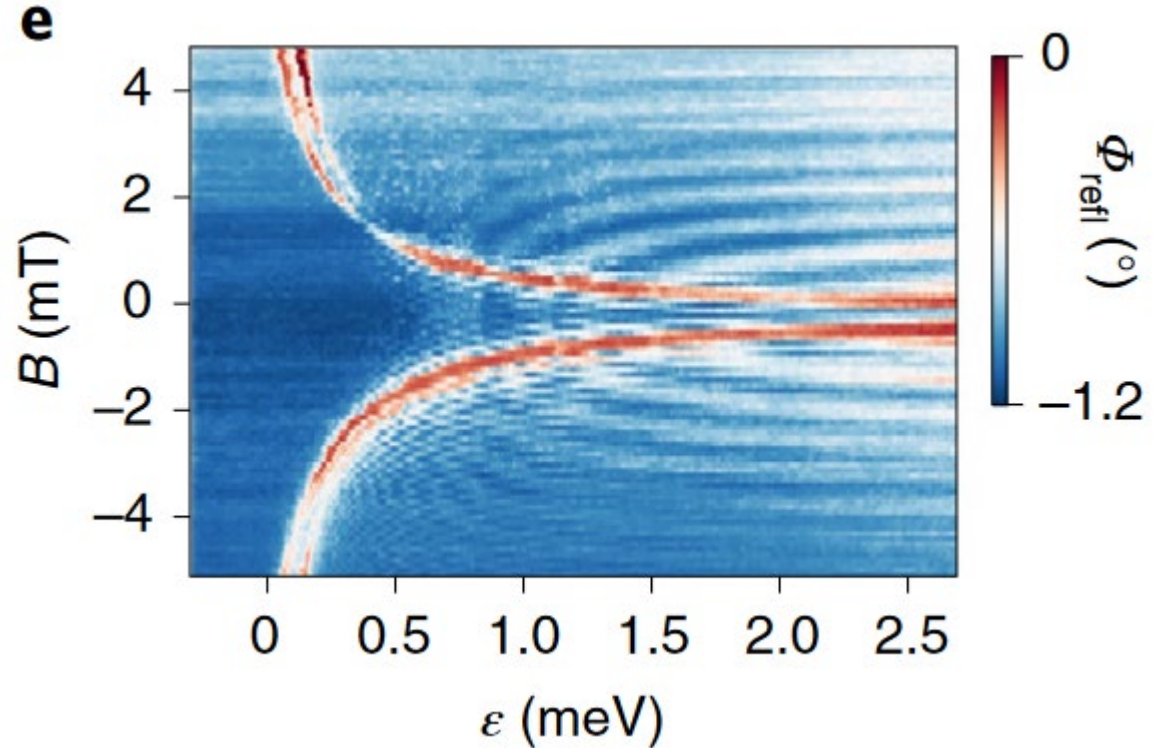
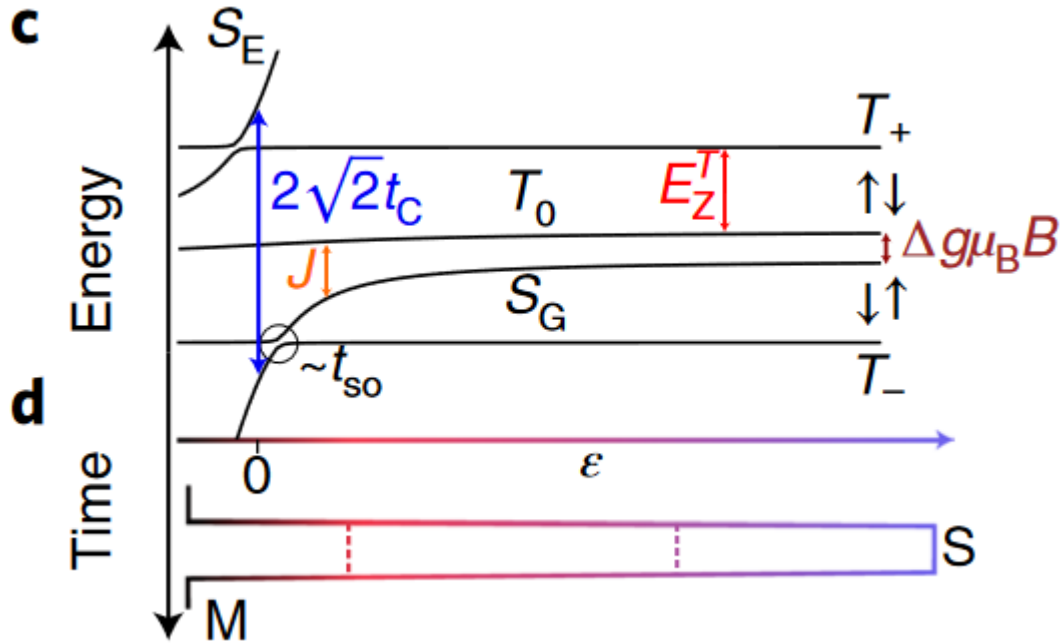


- Carrier density of $9.7 \times 10^{11} \text{cm}^{-2}$ without accumulation
- Boron dopants excluded from secondary ion mass spectroscopy; attribute to fixed negative charge in the oxide
- CB controls Δg and tunnel coupling t_c
- Pulses applied to LB+RB (affect mostly t_c , not Δg)

Operation region



Energy dispersion and spin funnel

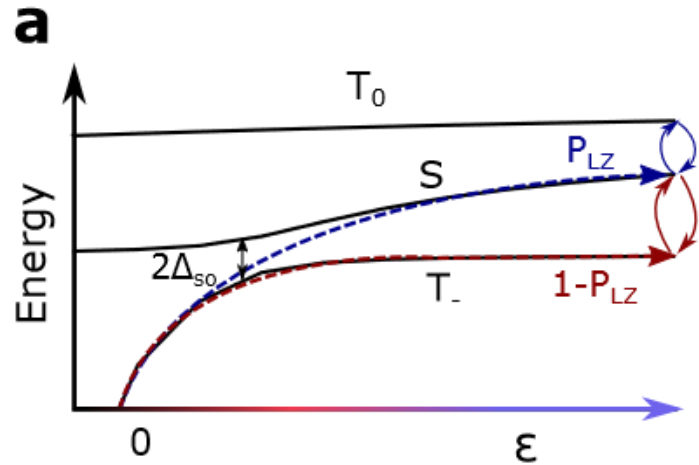


- Pulse sequence of **e**:

- Start in (2,0)
- Pulse to (1,1) at varying ε
- Pulse back to (2,0) after 100 ns

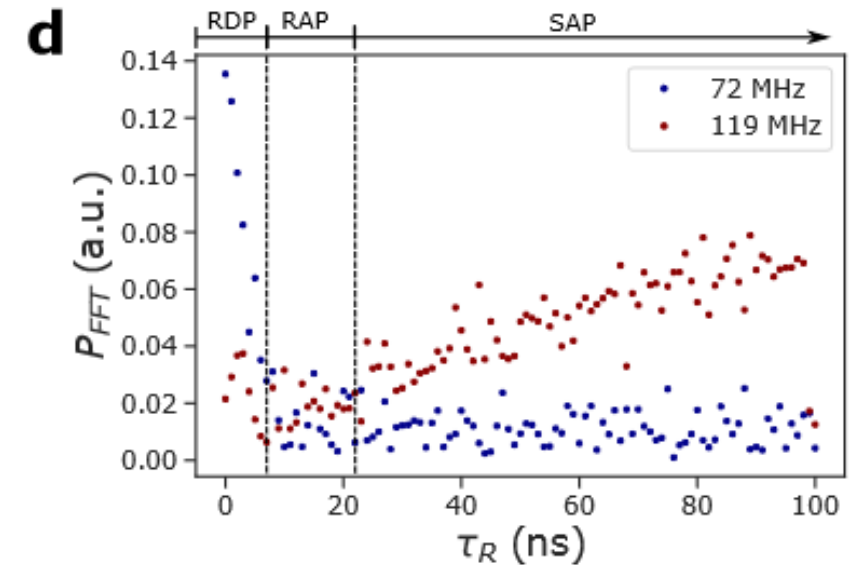
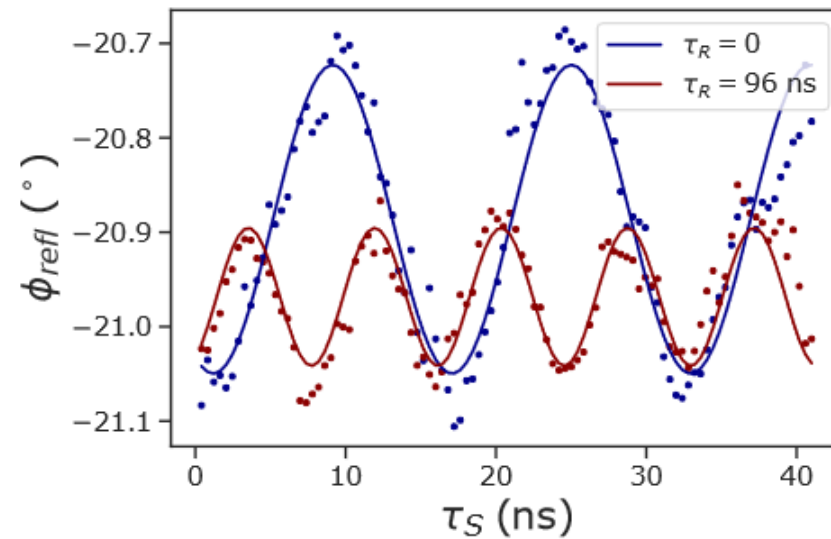
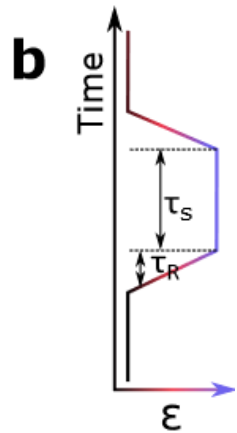
- Red line: $E_Z^T = J(\varepsilon)$
- Doubling due to SOI induced S- T_- oscillations
- S- T_0 oscillations at higher ε

Distinction between S-T₀ and S-T₋ oscillations

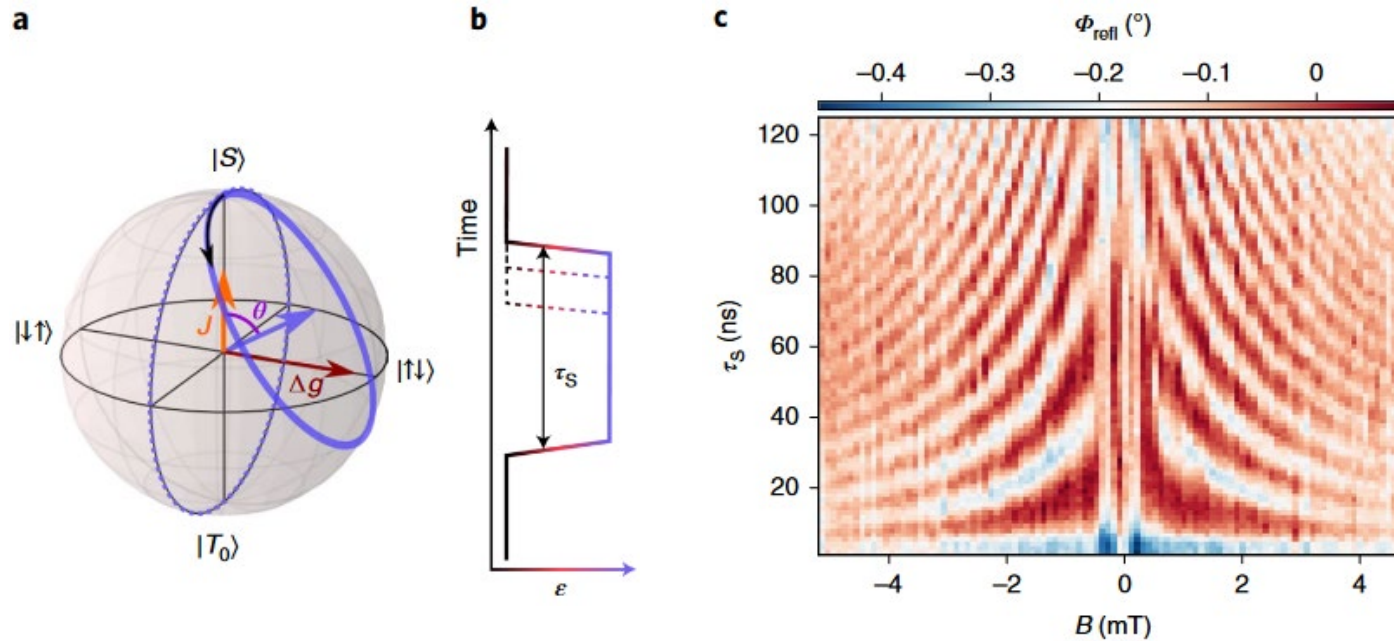


$$P_{LZ} = \exp\left\{-\frac{2\pi\Delta_{SO}^2}{\hbar v}\right\}$$

$$v = \frac{dE}{dt} = \frac{dE}{d\epsilon} \frac{d\epsilon}{dt}$$



Partial X rotations



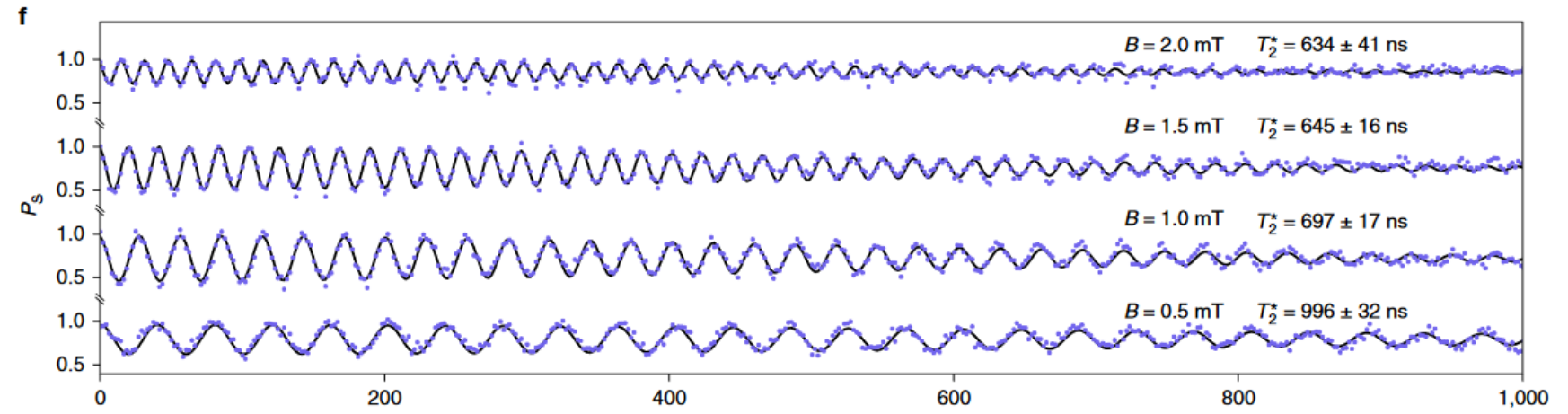
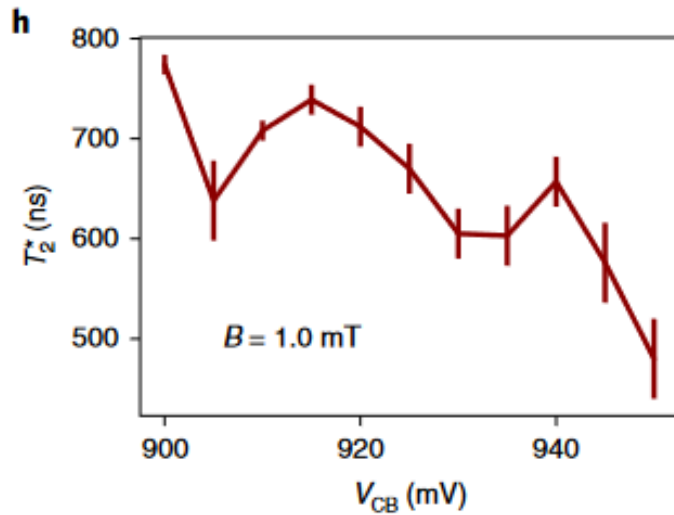
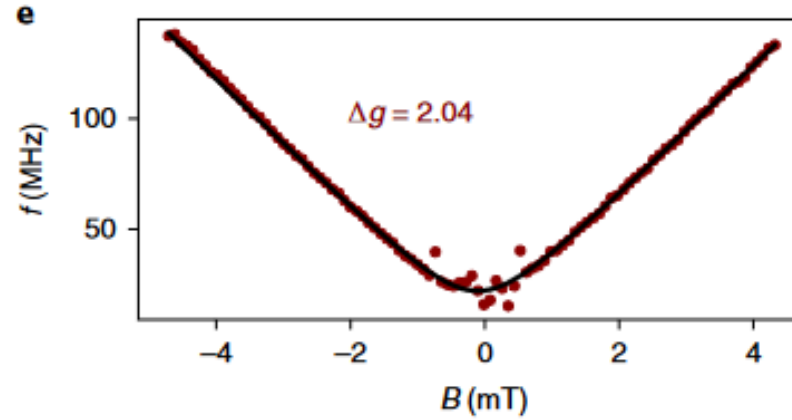
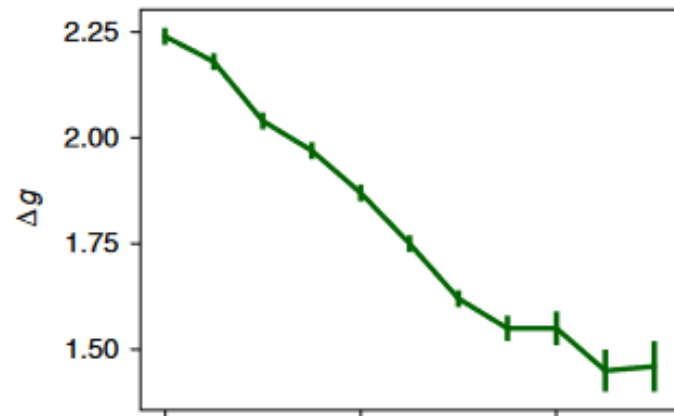
- Residual exchange coupling prevents ideal X rotations
- Actual rotation axis is:

$$\theta = \arctan\left(\frac{\Delta g \mu_B B}{J(\epsilon)}\right)$$

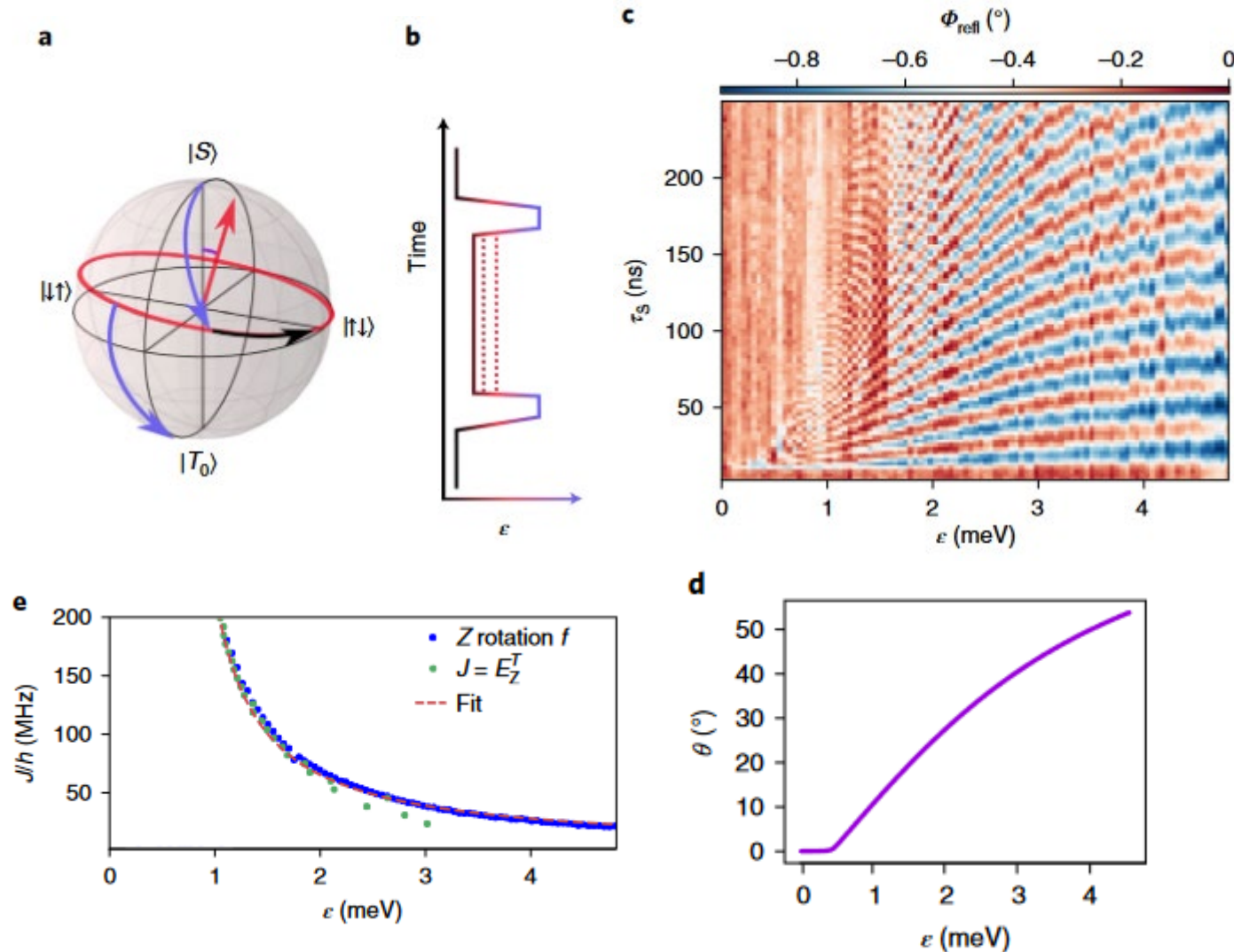
- Oscillations occur at frequency

$$f = \frac{1}{\hbar} \sqrt{J^2 + (\Delta g \mu_B B)^2}$$

Δg tunability



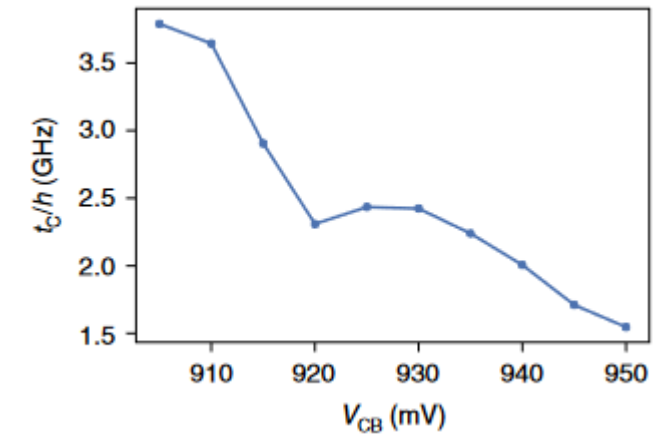
Complete X rotations and Z rotations



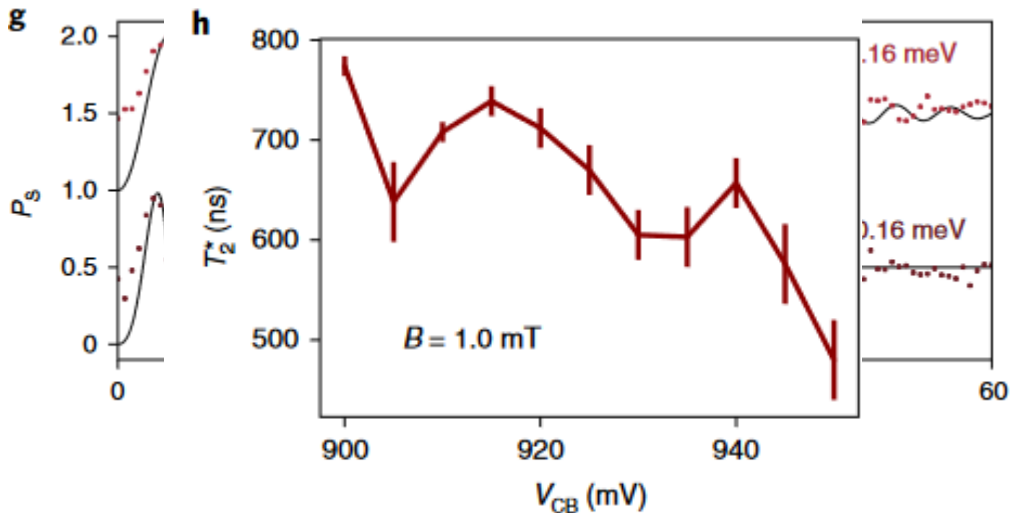
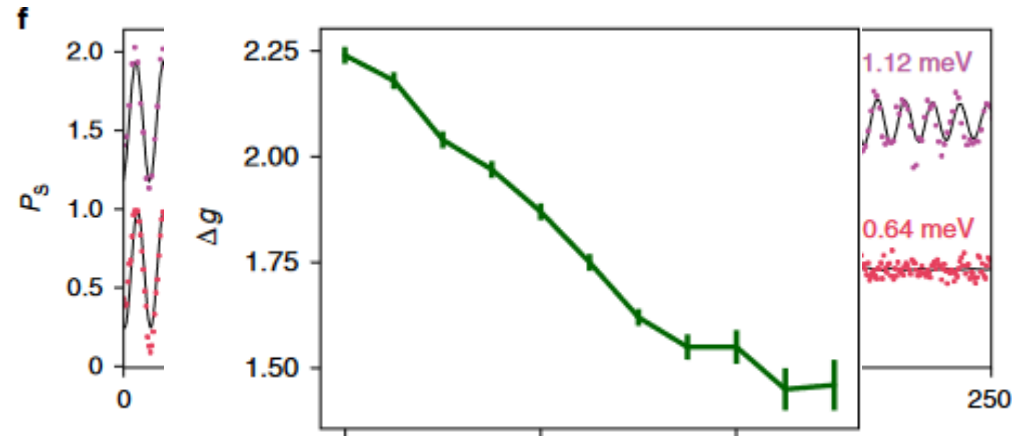
- Extract $J(\epsilon)$ from oscillation frequency and compare to spin funnel measurement

$$J(\epsilon) = \left| \frac{\epsilon}{2} - \sqrt{\frac{\epsilon^2}{4} + 2t_C^2} \right|$$

- Lines coincide for $\Sigma g = 11.0 \rightarrow g_L = 4.5, g_R = 6.5$
- Tunnel coupling t_C extracted as free fit parameter

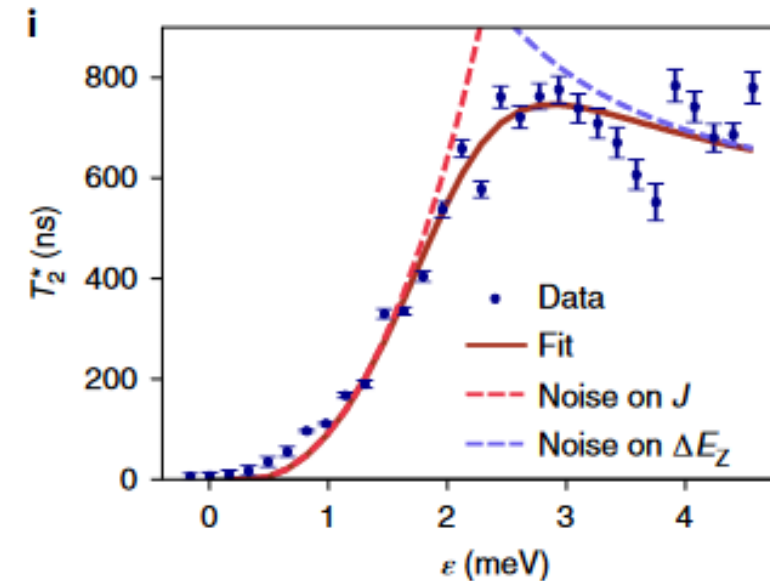


Complete X rotations and noise

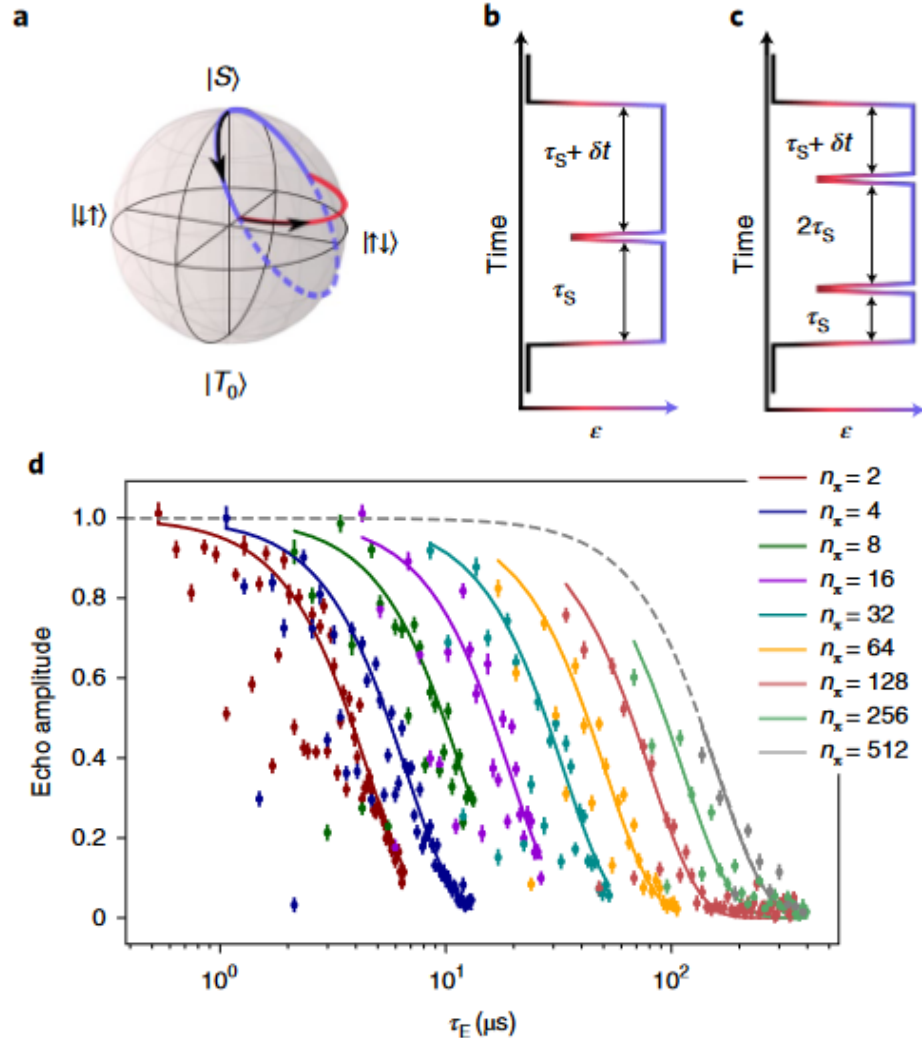


$$\frac{1}{T_2^*} = \frac{\pi\sqrt{2}}{h} \sqrt{\left(\frac{J(\epsilon)}{E_{\text{tot}}} \frac{dJ}{d\epsilon} \delta\epsilon_{\text{rms}}\right)^2 + \left(\frac{\Delta E_Z}{E_{\text{tot}}} \delta\Delta E_{Z,\text{rms}}\right)^2}$$

- Increase in Δg does not reduce T_2^* :
increase in t_C of 2 GHz \rightarrow increase of J
larger than ΔE_Z and $\Delta E_Z/E_{\text{tot}}$ is reduced

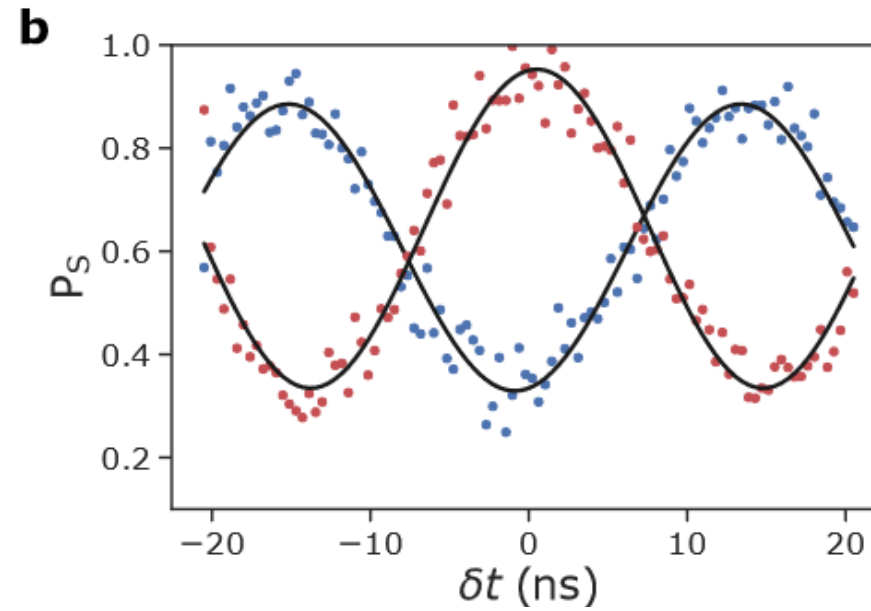
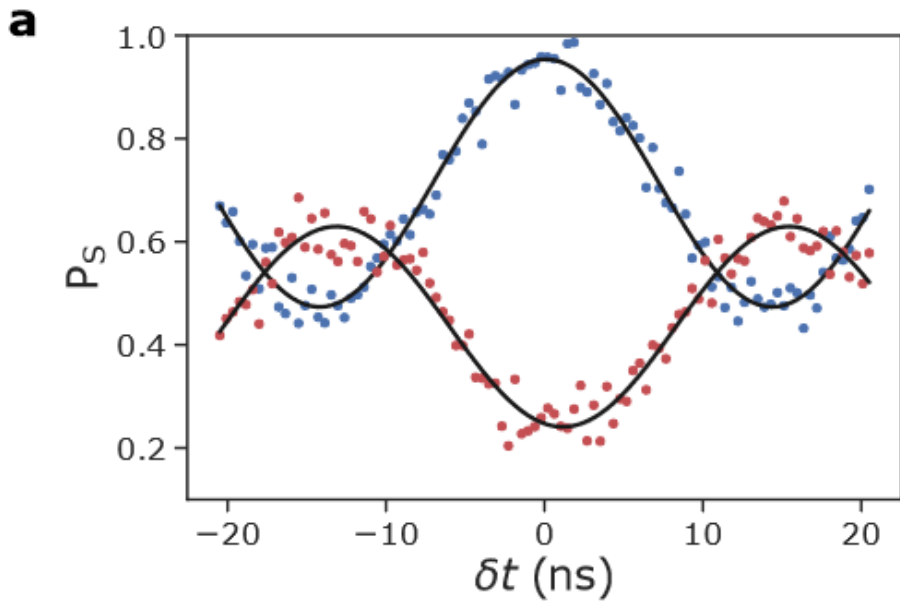


Refocusing pulses

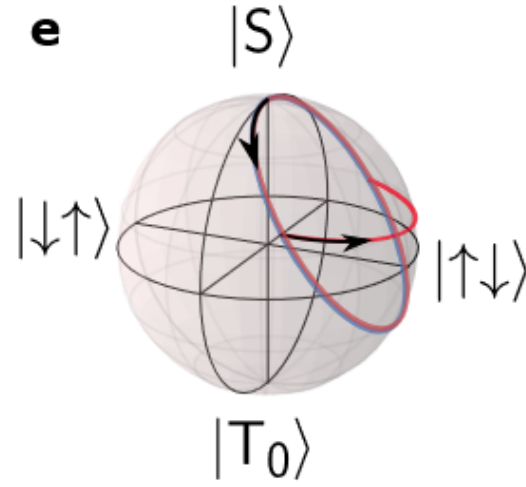
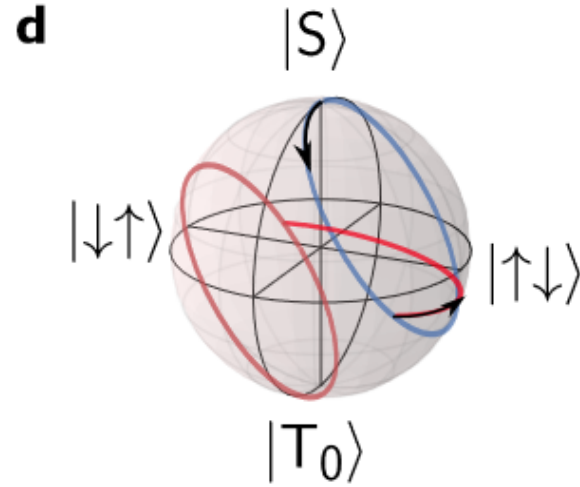
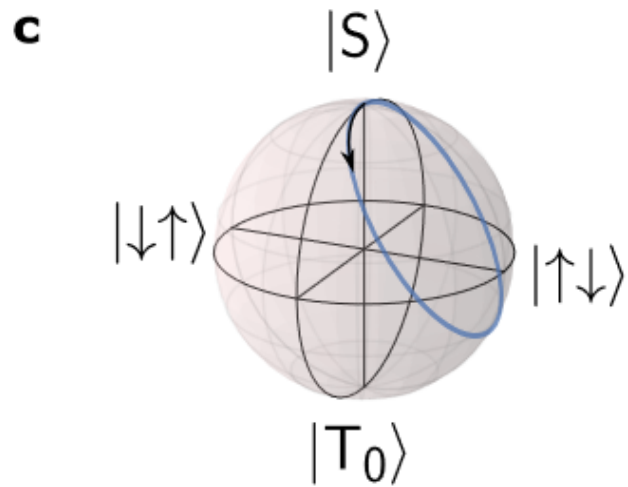


- Choose $\tau_S = (2n+1/2) * t_{\pi,x}$ to keep the system in the same state if no decoherence has occurred
- Calibration of refocusing pulse tricky, because J and Δg are never completely off
- Refocusing pulse needs to be applied in

Calibration of refocusing pulse



- Bad calibration in **a** and **d**
- Good calibration in **b** and **e**



Summary and outlook

Summary:

- Demonstration of two-axis control
- Dephasing time of $1 \mu\text{s}$ at $B=0.5 \text{ mT}$
- Electrically driven Δg rotations of 150 MHz at 5 mT
- Mostly low-frequency $1/f$ noise

Outlook:

- Move to latched or shelved readout:
 - improve visibility
 - operate at higher magnetic fields \rightarrow potentially surpass fastest Rabi frequencies